



HAL
open science

Tunneling spectroscopy of a single quantum dot coupled to a superconductor: From Kondo ridge to Andreev bound states

J D Pillet, P. Joyez, Rok Zitko, M F Goffman

► To cite this version:

J D Pillet, P. Joyez, Rok Zitko, M F Goffman. Tunneling spectroscopy of a single quantum dot coupled to a superconductor: From Kondo ridge to Andreev bound states. *Physical Review B: Condensed Matter and Materials Physics (1998-2015)*, 2013, 88 (4), pp.45101. 10.1103/PhysRevB.88.045101 . cea-01479207

HAL Id: cea-01479207

<https://cea.hal.science/cea-01479207>

Submitted on 28 Feb 2017

HAL is a multi-disciplinary open access archive for the deposit and dissemination of scientific research documents, whether they are published or not. The documents may come from teaching and research institutions in France or abroad, or from public or private research centers.

L'archive ouverte pluridisciplinaire **HAL**, est destinée au dépôt et à la diffusion de documents scientifiques de niveau recherche, publiés ou non, émanant des établissements d'enseignement et de recherche français ou étrangers, des laboratoires publics ou privés.



Tunneling spectroscopy of a single quantum dot coupled to a superconductor: From Kondo ridge to Andreev bound states

J.-D. Pillet,¹ P. Joyez,¹ Rok Žitko,² and M. F. Goffman^{1,*}

¹*Quantronics Group, Service de Physique de l'Etat Condensé, CNRS URA 2426, IRAMIS, CEA, F-91191 Gif-sur-Yvette, France*

²*J. Stefan Institute, Jamova 39, SI-1000 Ljubljana, Slovenia*

(Received 4 February 2013; published 1 July 2013)

We performed tunneling spectroscopy of a carbon nanotube quantum dot (QD) coupled to a metallic reservoir either in the normal or in the superconducting state. We explore how the Kondo resonance, observed when the QD's occupancy is odd and the reservoir is normal, evolves towards Andreev bound states (ABS) in the superconducting state. Within this regime, the ABS spectrum observed is consistent with a quantum phase transition from a singlet to a degenerate magnetic doublet ground state, in quantitative agreement with a single-level Anderson model with superconducting leads.

DOI: [10.1103/PhysRevB.88.045101](https://doi.org/10.1103/PhysRevB.88.045101)

PACS number(s): 74.45.+c, 73.23.-b, 73.21.La

I. INTRODUCTION

It is well established that in hybrid structures where a superconducting material (S) is put into contact with a non-superconducting one (X) the electron pairing correlations can propagate into X inducing superconductinglike properties near the interface, among which the ability to carry nondissipative currents (i.e., supercurrents). This phenomenon, known as the proximity effect, is truly generic: whatever the electronic properties of X , the proximity effect will occur, although possibly only in a range of the order of the interatomic distance in unfavorable cases.

Supercurrents transmitted through any S - X - S hybrid structure are the result of constructive interferences of pairs of electrons in X . As in an optical Fabry-Perot resonator, such constructive interferences occur only for discrete resonant electronic states confined inside X , known as the Andreev bound states (ABS).

A large variety of new hybrid nanostructures in which X is a semiconducting nanowire,¹ a single carbon nanotube,²⁻⁴ and a self-assembled semiconducting quantum dot (QD)⁵ have recently emerged. The interest in such new materials relies on the wealth of different phenomena they present (Kondo effect,^{6,7} spin-orbit coupling,⁸⁻¹⁰ Luttinger liquid behavior¹¹) and their interplay when coupled to superconducting reservoirs. Further interest in this field has been prompted by recent theoretical predictions on the existence of Majorana fermions at the edge of a S - X structure, where X is a one-dimensional semiconductor with strong spin-orbit interaction.^{12,13} Quantitatively understanding the proximity effect in these systems means understanding in detail how individual ABS form. This constitutes one of the central issues in the development of nanoscale hybrid superconducting circuits.

There is a wide range of experimental works on S - X - S structures that have explored the interplay between the Kondo effect and the formation of ABS in an indirect manner by measuring Josephson supercurrents or dissipative transport.^{6,7,14-18} In this work, instead of relying on transport through a QD, we perform tunneling spectroscopy of a single QD (coupled to a superconducting reservoir) in order to investigate this interplay in a direct way. In particular, we explore how the Kondo resonance, observed when the QD's occupancy is odd

and the reservoir is in the normal state, is replaced by ABS within the gap as the reservoir becomes superconducting. The ABS spectrum observed is consistent with a quantum phase transition from a singlet to a degenerate magnetic doublet ground state when the chemical potential of the QD is electrostatically swept, in quantitative agreement with a single-level Anderson model with superconducting electrodes.

II. TUNNELING SPECTROSCOPY

A. Sample fabrication and characterization

Carbon nanotubes (CNTs) have proved to be well suited for the observation of both Kondo effect^{6,7,14,18} and ABS⁴ because they fulfill three basic requirements: (i) At low enough temperatures (below 4 K) they behave as QDs whereby electron occupancy can be electrostatically tuned. (ii) Good S - X coupling with conventional superconductors (that can be turned into the normal state with a moderate magnetic field) were recently achieved,^{2,3} and (iii) there is a possibility of simultaneous weak coupling to a probe that allows tunneling spectroscopy of ABS.⁴

Devices were fabricated from individual carbon nanotubes (CNTs), grown by chemical vapor deposition on a 1 μm thick SiO_2 insulating layer atop a highly doped Si substrate used as a back gate (BG). Figure 1(a) shows a false-colored micrograph of a typical sample. The CNT is well connected to two superconducting metallic contacts 700 nm apart, leaving enough room to place a weakly coupled tunnel electrode in between them and a side gate (SG) [respectively in red and orange in Fig. 1(a)]. The electrodes are made of aluminum with a few nanometers of titanium as adhesion layer (as described elsewhere⁴) and are superconducting below ~ 1 K at zero magnetic field. The measurement of the differential conductance of the tunnel probe, $dI/dV(V)$, at low temperatures (35 mK) allows us to obtain the DOS of the CNT: when electrodes are in the normal state (applying a moderate magnetic field of ~ 0.05 T) $dI/dV(V)$ is proportional to the CNT DOS, with thermal broadening. When electrodes are in the superconducting state, the DOS can be obtained through a straightforward deconvolution procedure.⁴

Figure 2(a) presents the charge stability diagram obtained by measuring the CNT's tunneling DOS at the Fermi level of

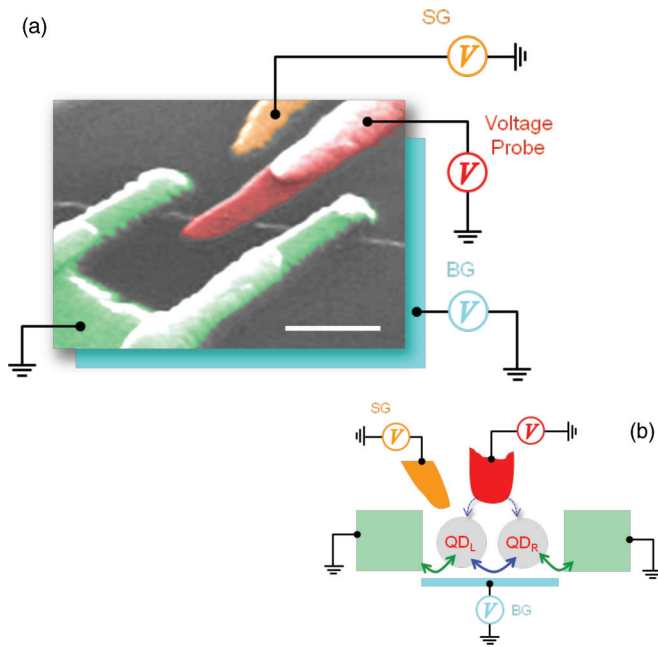


FIG. 1. (Color online) (a) Color-enhanced scanning electron micrograph (scale bar: 500 nm) of a device fabricated for the tunneling spectroscopy of a carbon nanotube (CNT). The substrate consists of highly doped silicon serving as a back gate (BG), shown here in cyan, with a 1 μm surface oxide layer. A second gate electrode [side gate (SG)] is used to electrostatically influence the left part the CNT. A grounded aluminum fork (green) is well connected to the CNT. The measurement of dI/dV through the tunnel probe (red) gives access to the DOS in the CNT. (b) Schematic representation of the system: the presence of the tunnel probe electrode likely acts as a scatterer splitting the CNT into two QDs.

the electrodes ($V = 0$ on the probe) in the normal state as a function of the side gate (SG) and back gate (BG) voltage. One can distinguish large black areas where the DOS is close to zero and bright lines that appear each time the chemical potential of the CNT crosses the Fermi level.

These lines run mainly in two directions [orange and cyan dashed lines in Fig. 2(a)] and show avoided crossings. The pattern observed is consistent with two coupled quantum dots as depicted in Fig. 1(b): In both directions, adjacent pairs of parallel lines, which are close (far) apart delimit regions where occupancy of one of the dots is odd (even). Hence, the largest black diamonds define regions where both dots are in an even configuration. The distance between lines is proportional to the addition energy: for odd occupancy valleys it corresponds to the charging energy $U_{L(R)}$ while for even valleys it corresponds to $U_{L(R)} + \delta E_{L(R)}$ ($\delta E_{L(R)}$ being the energy difference between orbitals of the QD). The coupling between dots is manifested by the anticrossing observed between these lines. The sharpness of the lines reflects the strength of the coupling of each QD to the respective electrode reservoir: from weak (thin sharp bright lines) to strong (fuzzy lines). Note that sometimes close pairs of lines strongly overlap forming a single fuzzy band. As we will see in the next section, this is related to the Kondo resonance developed in odd valleys. The ensemble of these results unambiguously shows that the central probe electrode also acts as an efficient scatterer, hence

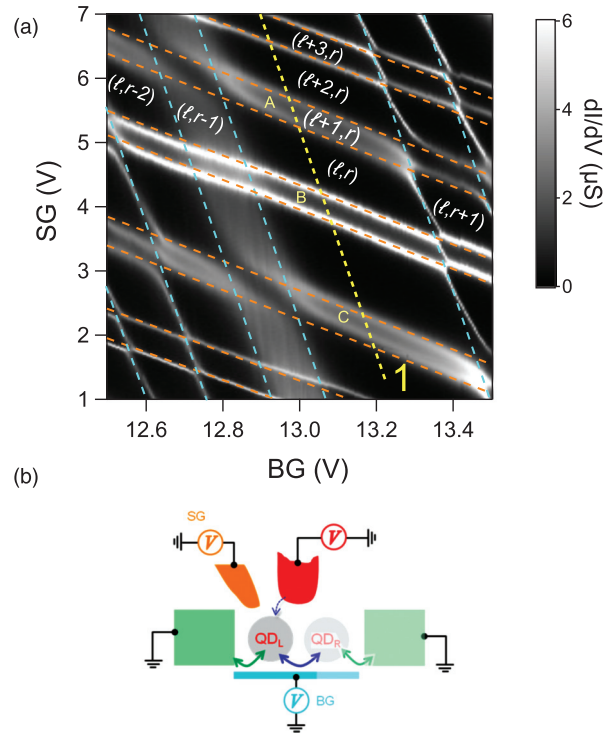


FIG. 2. (Color online) (a) Density plot of the CNT DOS measured, in the normal state ($B \sim 0.05$ T), at zero probe voltage as a function of SG (vertical axis) and BG (bottom axis). Superimposed dotted thin lines are guides to the eyes showing the electronic levels of two isolated QDs. Orange (cyan) lines correspond to resonances of the left (right) QD. Between these dotted lines, each diamond is indexed by a pair of integer numbers, which denote the equilibrium charge on left and right dot. Here the labeling is such that ℓ and r are even numbers. Avoided crossings reveal the interdot coupling. (b) Schematic of the experiment testing the DOS of a single QD (QD_L): by following a trajectory in the (SG, BG) plane that keeps QD_R in a “Coulomb blocked” even state [dashed yellow line 1 in (a)], the tunnel current is forced to solely go through QD_L giving access to its DOS. Dashed yellow line 1 indicates the trajectory followed to explore the DOS of a single QD in the normal and in the superconducting state shown in Figs. 3(a) and 3(b) respectively. A, B, and C correspond to the odd valleys analyzed.

confirming the hypothesis we made in a previous work.⁴ Broadly, the system we report here is the realization of a tunable double quantum dot with integrated DOS readout. In what follows we demonstrate that each QD can be fully characterized both in the normal and in the superconducting state thus enabling to directly address the interplay between the Kondo effect and superconductivity, and the resulting formation of ABS.

B. Single quantum dot behavior

The stability diagram of Fig. 2(a) shows that one can explore in principle different regimes of the double QDs system by suitably adjusting SG and BG. In particular one can individually characterize each single QD: by simultaneously tuning SG and BG and following the trajectory depicted in Fig. 2(a) (yellow line denoted as 1) we set the right QD (QD_R) in a Coulomb blocked even state. As a consequence,

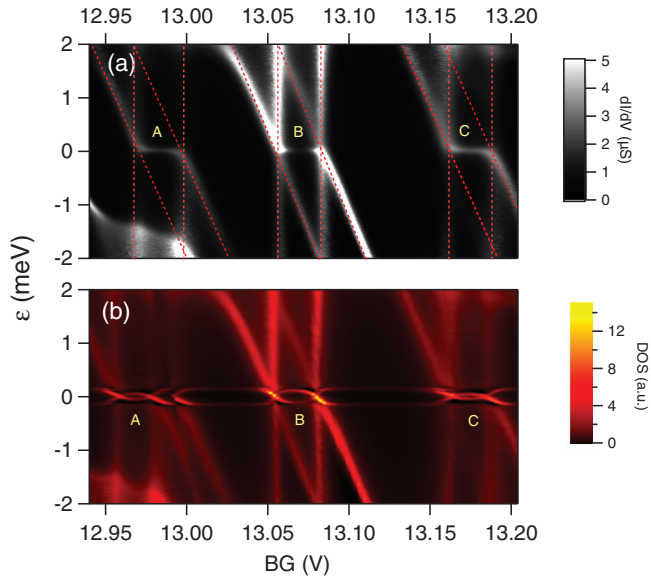


FIG. 3. (Color online) (a) Density plot of CNT's tunneling DOS in the normal state as a function of voltage probe V (vertical axis) and BG (horizontal axis) following line 1 in the plane (BG, SG) depicted in Fig. 2(a), after correcting for the gating effect of the probe junction. Odd valleys A, B, C show the development of a Kondo ridge. From the size of the diamonds (delimited by dashed red thin lines) the charging energy can be estimated. (b) Same as (a) in the superconducting state. Around the Fermi level, the superconducting gap ($\Delta = 150 \pm 5 \mu\text{eV}$) develops and ABS are observed. By sweeping gate voltages along line 1, ABS form loops of different sizes each time an odd valleys is crossed.

the tunnel current will flow essentially through the QD_L and the measurement of $dI/dV(V)$ will give access to its DOS. Analogously, the DOS of QD_R can be obtained by setting QD_L in a Coulomb blocked even state.

Figure 3 shows the DOS of QD_L both in the normal and in the superconducting state as a function of the energy at which quasiparticles are injected (left axis) and BG voltage (bottom axis). Note that SG is simultaneously swept in order to follow line 1 [see Fig. 2(a)]. In the normal state [Fig. 3(a)] we observe the well known Coulomb blockade diamond pattern, highlighted with red dashed lines, alternating in size between large and small as BG is swept, consistent with a broken valley degeneracy. This clearly identifies an odd (even) number of quasiparticles in the QD in the small (large) diamond. From this graph we extracted the Coulomb repulsion energy U for each odd valley: $U_A = 2.0 \pm 0.1 \text{ meV}$, $U_B = 2.05 \pm 0.1 \text{ meV}$ and $U_C = 1.9 \pm 0.1 \text{ meV}$ and we estimated the level spacing $\sim 2 - 2.5 \text{ meV}$. The last value is consistent with the usual estimation:¹⁹ $\delta E \sim 0.5 \text{ eV}/L(\text{nm})$ considering the CNT QD of size $L \simeq 300 \text{ nm}$. Moreover, odd valleys (A, B, C) present a zero bias peak that reveals the Kondo effect. In each odd valley the intensity of this peak varies, reflecting that the associated Kondo energy $k_B T_K$ is different as electronic orbitals couple differently to the reservoir.

Figure 3(b) shows the superconducting Coulomb diamond pattern. Tunneling DOS shows how ABS develop around the Fermi energy. By sweeping gate voltages along line 1, ABS form loops of different sizes in each odd valley. In even valleys,

ABS merge with the superconducting gap edge (estimated to be $\Delta = 150 \pm 5 \mu\text{eV}$). For energies $\varepsilon \gg \Delta$, the tunneling DOS is the same as the one measured in the normal state. The discontinuity at the right-hand side of valley A is due to a change of the offset charge of the QD and merely shifts its electrostatic potential. As a result, the intrinsic energies and resonances are not altered and a comparison between the normal and the superconducting behavior for valley A is still valid. In the next section we develop a model that allows us to quantitatively account for the behavior observed both in the normal and in the superconducting state.

III. ANDERSON IMPURITY MODEL

The minimal model for a QD coupled to a metallic reservoir in the regime where δE is sufficiently large to restrict the analysis to a single spin-degenerate orbital is provided by a single-level Anderson impurity model (AIM),²⁰ with a Hamiltonian $H = H_R + H_{QD} + H_T$ where H_{QD} corresponds to the uncoupled quantum dot given by

$$H_{QD} = \varepsilon_0(n_\uparrow + n_\downarrow) + U n_\uparrow n_\downarrow, \quad (1)$$

where $n_\sigma = d_\sigma^\dagger d_\sigma$ and d_σ^\dagger creates an electron with spin σ in the QD orbital located at ε_0 . The energy U is the local Coulomb interaction for two electrons with opposite spin inside the single orbital of the QD. The metallic reservoir is described by H_R , usually represented by a Bardeen-Cooper-Schrieffer mean-field Hamiltonian of the type

$$H_R = \sum_{k,\sigma} \varepsilon_k c_{k,\sigma}^\dagger c_{k,\sigma} + \sum_k (\Delta c_{k,\uparrow}^\dagger c_{-k,\downarrow}^\dagger + \text{H.c.}), \quad (2)$$

where $c_{k,\sigma}^\dagger$ creates an electron with spin σ at the single particle energy level ε_k of the reservoir, referred to its chemical potential ($\varepsilon_k = \epsilon_k - \mu$) and Δ is the superconducting order parameter. The normal-state behavior is recovered by setting $\Delta = 0$. Finally, H_T describes the coupling between the reservoir and the QD and has the form

$$H_T = \sum_{k,\sigma} (V_k c_{k,\sigma}^\dagger d_\sigma + \text{H.c.}). \quad (3)$$

This last term is usually simplified by considering that the normal-state density of the reservoir ρ is constant in the range of energies around the Fermi level of the order of Δ and by neglecting the k dependence of the hopping elements $V_k \simeq V$ within this range. The coupling between the reservoir and the QD is then characterized by a single parameter $\Gamma = \pi \rho |V|^2$.

To obtain the normal and superconducting exact tunneling spectrum of the system we solved the above Hamiltonian in the NRG approach^{21,22} using the NRG-LJUBLJANA code.²³ The results obtained reproduced previously reported calculations.²² When the QD is tuned in an odd valley, the system has two possible ground states (GSs): a magnetic doublet ($S = \frac{1}{2}$) or a singlet ($S = 0$). The nature of the singlet has two well-known limiting cases: BCS-like ABS (i.e., a superposition of a zero and double occupancy) or Kondo-like bound state (i.e., a many-body state where the QD's spin is screened by electrons from the metallic reservoir near the Fermi energy), although there is no definite boundary between them.²² The actual GS is determined by the magnitude of the Kondo energy $k_B T_K$ (which is a function of U , Γ and ε_0 ²⁴⁻²⁷) with respect to Δ . For

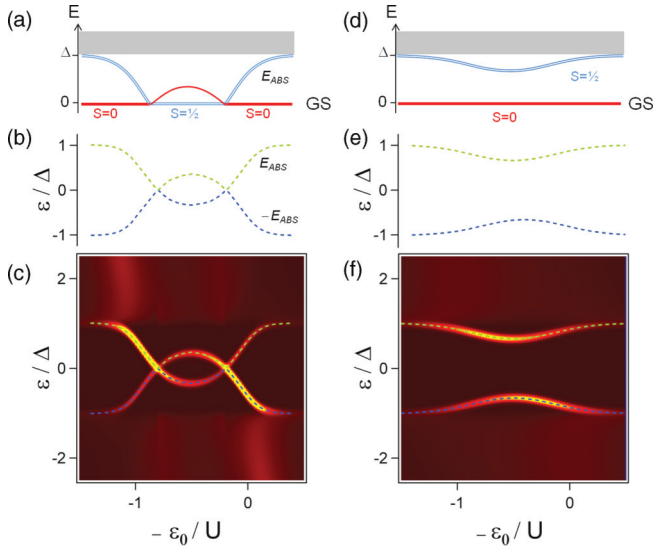


FIG. 4. (Color online) Schematic of the excitation spectrum of the S-QD for (a) $\Gamma/\Delta \lesssim 1$ and (d) $\Gamma/\Delta \gg 1$: Andreev transitions correspond to the excitation between the GS and excited state by addition of an electron or a hole [respectively blue and green dashed lines in (b) and (e)] at an energy $|E_{\text{ABS}}|$ relative to the GS. The singlet ($S = 0$) and spin degenerate doublet ($S = \frac{1}{2}$) regions are indicated (red and double blue lines respectively). When $E_{\text{ABS}} = 0$ a quantum phase transition takes place, accompanied by an abrupt change in the spectral weights of ABS [see (c)]. (c) and (f) Color plot of the DOS spectrum for $U/\Delta = 13.3$ and $\Gamma/\Delta = 0.9, 5$ [(c) and (f), respectively] as a function of the energy (left axis) and the chemical potential of the QD (bottom axis). The sharp resonances observed within Δ are artificially broadened to make them visible.

$k_B T_K \gg \Delta$, calculations show that the GS is the singlet. In the opposite limit, $k_B T_K \ll \Delta$, the doublet is the GS because the formation of the Kondo-like (BCS-like) singlet is hampered by the lack of states in the vicinity of the Fermi energy (charging

energy associated with the double occupancy of the dot). The GS transition between singlet and doublet is predicted to occur when $k_B T_K \approx \Delta$.^{25–27} When the QD is tuned in an even valley, the GS is always singlet.

IV. FITTING THE TUNNELING SPECTRUM WITH THE AIM

In our experiments $U \sim 2$ meV is estimated from the normal-state spectrum in each odd valley, $\Delta \sim 0.15$ meV is obtained from the superconducting data and the chemical potential (ε_0) of the QD is varied by sweeping gate voltages. The sole free parameter is the coupling Γ between the QD and the corresponding electron reservoir. In the case of our experiment ($U/\Delta \gtrsim 10$) the calculations show that when sweeping the chemical potential of the QD across an odd valley, the GS transition between singlet and doublet occurs provided that $\Gamma/\Delta \lesssim 1$. Figures 4(a) and 4(d) display the evolution of the first excited state and the nature of the GS as a function of the chemical potential when such transition occurs ($\Gamma/\Delta < 1$) or not ($\Gamma/\Delta \gg 1$), respectively.

Tunneling spectroscopy consists in injecting or extracting electrons and this has mainly two consequences: first, it may only reveal transitions between the GS and excited states whose spin differ by $1/2$. With the parameters of our experiment, there is only one such possible transition within the superconducting gap; we call it the Andreev transition and call its energy E_{ABS} . Second, since the singlet state is an electron-hole superposition, tunneling spectrum will show mirrored resonances at energies $\pm |E_{\text{ABS}}|$ [Figs. 4(b) and 4(e)] with intensities that reflect respectively the hole and electron content [Figs. 4(c) and 4(f)].

The seeming crossing of resonances at the Fermi energy in Fig. 4(c) marks the GS transition: before and after the “loop” the GS is a spin singlet ($S = 0$), inside the loop region it becomes a magnetic doublet. This transition is accompanied

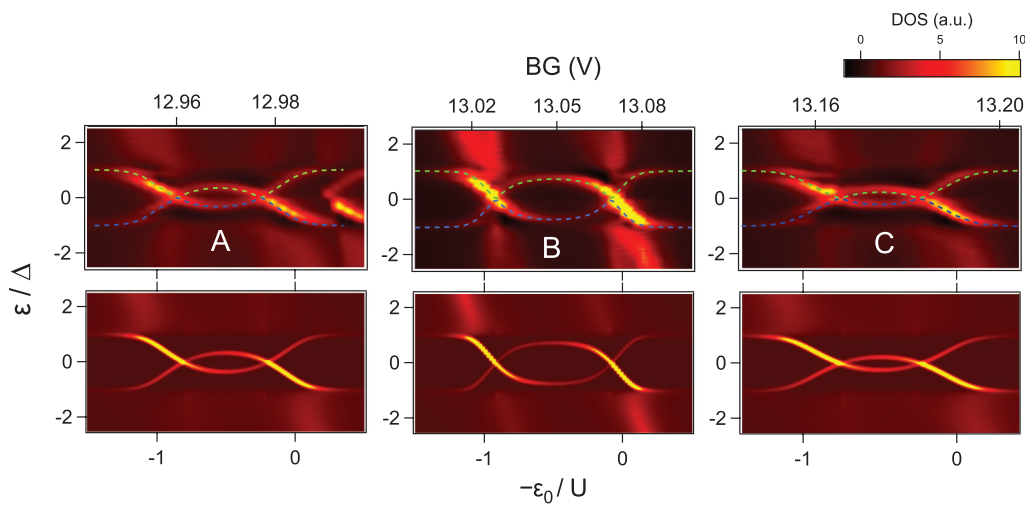


FIG. 5. (Color online) Top: Color plot of CNT’s tunneling DOS measured in the superconducting state as a function of energy (left axis) and BG voltage (top axis) in odd valley A, B, and C. By using the proportionality factor that converts BG into energy, BG can be expressed as the dot level position ε_0 (bottom axis) used in the model described in the text. Green and blue dashed lines are the Andreev transitions obtained from the NRG calculation shown at the bottom: DOS spectrum of the QD calculated by a NRG algorithm using U and Δ obtained from the experiments ($U/\Delta = 13.3, 13.6, 12.7$ for A, B, and C, respectively) and Γ as a sole fitting parameter ($\Gamma/\Delta = 1.6, 0.86, 1.7$ for A, B, and C, respectively). Andreev transitions were artificially broadened to make them visible.

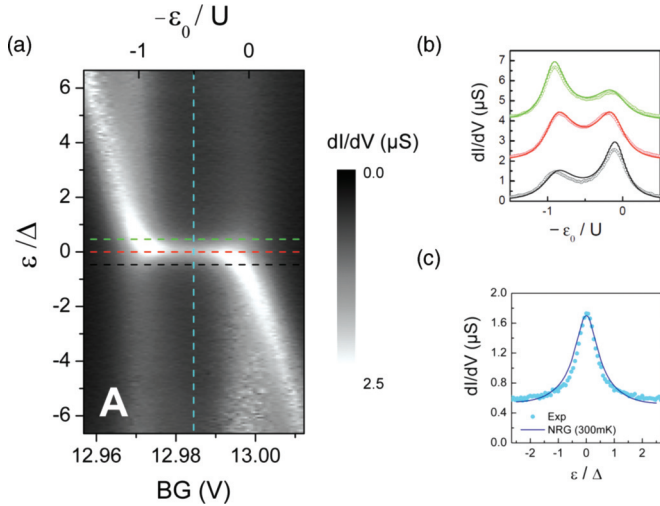


FIG. 6. (Color online) (a) Color plot of tunneling DOS measured in the normal state as a function of energy (left axis) and BG voltage (bottom axis) in odd valley A. (b) Tunneling DOS at $\varepsilon/\Delta = -0.47$ (black), 0 (red), and 0.47 (green) as a function of the level position ε_0 . Solid lines: NRG calculation using the parameter $\Gamma/\Delta = 0.86$ obtained when fitting the superconducting state. (c) Tunneling DOS at the electron-hole symmetry point ($\varepsilon_0/U = -0.5$) as a function of the energy. Solid line: NRG calculation using the parameter $\Gamma/\Delta = 0.86$ obtained when fitting the superconducting state.

by an abrupt change in the spectral weights [see Fig. 4(c)]. The tunneling spectrum pattern shown in Fig. 4(c) is similar to the one observed in each odd valley presented in Fig. 3(b) showing that at the center of each odd valley investigated the GS is a magnetic doublet. For a given U , the size of the loop is governed by the parameter Γ . For each odd valley presented in Fig. 3(b) we adjusted Γ in order to fit the size of the loop observed. The agreement between experiment and NRG calculations is quantitative in the whole range as shown in Fig. 5.

Using the same values of Γ obtained for each odd valley investigated, we calculated the spectrum in the normal state. Figure 6(a) shows a close up of the data taken at the odd valley A in the normal state and Figs. 6(b) and 6(c) present four

different profiles as a function of ε_0 (keeping ε constant) and ε (at $\varepsilon_0 = -U/2$) respectively. Solid lines correspond to the NRG calculations using Γ obtained in the superconducting state. A quantitative agreement is obtained if we consider a temperature of 300 mK in the calculation, instead of the actual temperature of the sample (35 mK). This effect could be ascribed to a broadening of the measured DOS due to the finite coupling of the probe and the QD.

V. CONCLUSION

In summary, we report the realization of a tunable double quantum dot with integrated DOS readout. We demonstrate that each QD can be fully characterized both in the normal and in the superconducting state. In particular, we explore how the Kondo resonance, observed when the QD's occupancy is odd and the reservoir is normal, evolves toward ABS. The tunneling spectrum forms loops of different sizes each time an odd valley is crossed. This behavior is consistent with a quantum phase transition from a singlet to a degenerate magnetic doublet ground state when the chemical potential of the QD is electrostatically swept, in good quantitative agreement with the Anderson impurity model presented. As a result, ABS spectroscopy constitutes a new tool to quantitatively account for the coupling Γ between the QD and the metallic reservoir. More generally, the system presented here together with the individual characterization of each QD can serve as starting point for exploring quantitatively the rich physics of the proximity effect in a double quantum dot system and testing proposed models.²⁸ Furthermore, the ABS spectroscopy experiment we present can constitute a robust test of the different proposals in systems where superconductivity becomes topological as recently suggested.²⁹

ACKNOWLEDGMENTS

We thank A. Levy Yeyati for enlightening discussions. We gratefully acknowledge help from other members of the Quantronics Group, in particular P. Senat and P. F. Orfila for invaluable technical assistance. This work was partially funded by ANR through project MASH.

*Corresponding author: marcelo.goffman@cea.fr

¹J. A. van Dam, Y. V. Nazarov, E. P. A. M. Bakkers, S. D. Franceschi, and L. P. Kouwenhoven, *Nature (London)* **442**, 667 (2006).

²A. Y. Kasumov, R. Deblock, M. Kociak, B. Reulet, H. Bouchiat, I. I. Khodos, Y. B. Gorbatov, V. T. Volkov, C. Journet, and M. Burghard, *Science* **284**, 1508 (1999).

³P. Jarillo-Herrero, J. A. van Dam, and L. P. Kouwenhoven, *Nature (London)* **439**, 953 (2006).

⁴J.-D. Pillet, C. H. L. Quay, P. Morin, C. Bena, A. Levy Yeyati, and P. Joyez, *Nature Phys.* **6**, 965 (2010).

⁵R. S. Deacon, Y. Tanaka, A. Oiwa, R. Sakano, K. Yoshida, K. Shibata, K. Hirakawa, and S. Tarucha, *Phys. Rev. Lett.* **104**, 076805 (2010).

⁶J.-P. Cleuziou, W. Wernsdorfer, V. Bouchiat, T. Ondarçuhu, and M. Monthieux, *Nature Nanotech.* **1**, 53 (2006).

⁷C. Buizert, A. Oiwa, K. Shibata, K. Hirakawa, and S. Tarucha, *Phys. Rev. Lett.* **99**, 136806 (2007).

⁸F. Kuemmeth, S. Ilani, D. C. Ralph, and P. L. McEuen, *Nature (London)* **452**, 448 (2008).

⁹T. S. Jespersen, K. Grove-Rasmussen, J. Paaske, K. Muraki, T. Fujisawa, J. Nygård, and K. Flensberg, *Nature Phys.* **7**, 348 (2011).

¹⁰S. Nadj-Perge, V. S. Pribiag, J. W. G. van den Berg, K. Zuo, S. R. Plissard, E. P. A. M. Bakkers, S. M. Frolov, and L. P. Kouwenhoven, *Phys. Rev. Lett.* **108**, 166801 (2012).

¹¹M. Bockrath, D. H. Cobden, J. Lu, A. G. Rinzler, R. E. Smalley, L. Balents, and P. L. McEuen, *Nature (London)* **397**, 598 (1999).

¹²R. M. Lutchyn, J. D. Sau, and S. Das Sarma, *Phys. Rev. Lett.* **105**, 077001 (2010).

- ¹³Y. Oreg, G. Refael, and F. von Oppen, *Phys. Rev. Lett.* **105**, 177002 (2010).
- ¹⁴M. R. Buitelaar, T. Nussbaumer, and C. Schönberger, *Phys. Rev. Lett.* **89**, 256801 (2002).
- ¹⁵H. I. Jørgensen, T. Novotný, K. Grove-Rasmussen, K. Flensberg, and P. E. Lindelof, *Nano Lett.* **7**, 2441 (2007).
- ¹⁶A. Eichler, M. Weiss, S. Oberholzer, C. Schönberger, A. Levy Yeyati, J. C. Cuevas, and A. Martín-Rodero, *Phys. Rev. Lett.* **99**, 126602 (2007).
- ¹⁷A. Eichler, R. Deblock, M. Weiss, C. Karrasch, V. Meden, C. Schönberger, and H. Bouchiat, *Phys. Rev. B* **79**, 161407 (2009).
- ¹⁸R. Maurand, T. Meng, E. Bonet, S. Florens, L. Marty, and W. Wernsdorfer, *Phys. Rev. X* **2**, 011009 (2012).
- ¹⁹M. Bockrath, D. H. Cobden, P. L. McEuen, N. G. Chopra, A. Zettl, A. Thess, and R. E. Smalley, *Science* **275**, 1922 (1997).
- ²⁰P. W. Anderson, *Phys. Rev.* **124**, 41 (1961).
- ²¹K. G. Wilson, *Rev. of Mod. Phys.* **47**, 773 (1975).
- ²²J. Bauer, A. Oguri, and A. C. Hewson, *J. Phys.: Condens. Matter* **19**, 486211 (2007).
- ²³R. Žitko, NRG LJUBLJANA code for numerical renormalization group calculations, <http://nrgljubljana.ijs.si/>.
- ²⁴F. D. M. Haldane, *Phys. Rev. Lett.* **40**, 416 (1978).
- ²⁵K. Satori, H. Shiba, O. Sakai, and Y. Shimizu, *J. Phys. Soc. Jpn* **61**, 3239 (1992).
- ²⁶M.-S. Choi, M. Lee, K. Kang, and W. Belzig, *Phys. Rev. B* **70**, 020502 (2004).
- ²⁷F. Siano and R. Egger, *Phys. Rev. Lett.* **93**, 047002 (2004).
- ²⁸R. Žitko, M. Lee, R. López, R. Aguado, and M. S. Choi, *Phys. Rev. Lett.* **105**, 116803 (2010).
- ²⁹D. Chevallier, D. Sticlet, P. Simon, and C. Bena, *Phys. Rev. B* **85**, 235307 (2012).